Supplement of Geosci. Model Dev., 12, 2607–2633, 2019
https://doi.org/10.5194/gmd-12-2607-2019-supplement

Geoscientific Model Development
Open Access

Supplement of

Implementation of an immersed boundary method in the Meso-NH v5.2 model: applications to an idealized urban environment

Franck Auguste et al.

Correspondence to: Franck Auguste (franck.auguste@cerfacs.fr)

The *Implementation of an immersed boundary method in the Meso-NH v5.2 model: Applications to an idealized urban-like environment* paper is enriched with a viscous buoyancy-driven flow case (Straka et al., 1993). This additional case presents the comparison of the results obtained by a Boundary-Fitted Method (BFM) and Immersed-Boundary Method (IBM) used in the Meso-NH (MNH) code (Lafore et al., 1998; Lac et al., 2018). This case induces an IB forcing of the energy equation (see Eq. 1 of the main paper). The popular and thermodynamic case proposed by Straka et al. (1993) is a cold air bubble falling in an idealized atmospheric condition and followed in time by the development of a gravity current above an ideal surface. This case with MNH-BFM was intensively investigated in Lunet et al. (2017) to compare a fifth-order WENO advection scheme to a fourth centered scheme (CEN4), the two showing a good agreement with the literature. In this study, only CEN4 is employed.

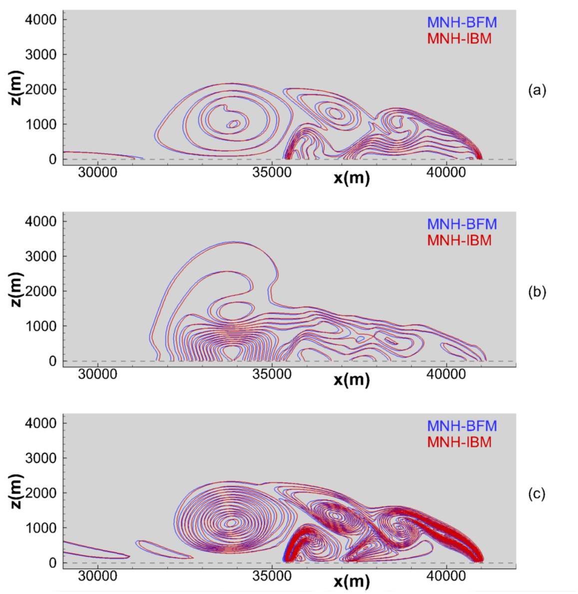

Figure S1. *The Straka density current developed at $t = 900$ s:* **(a)** *sixteen isocontours of the potential temperature $\theta \in [284 : 299]$ K;* **(b)** *the kinetic energy where $e_k \in [0 : 660]$ $m^2 s^{-2}$;* **(c)** *the enstrophy where $e_s \in [0 : 0.0064]$ s^{-2}. The blue (red) line corresponds to the MNH-BFM (MNH-IBM) solutions with $\Delta x = 50$ m.*

Case description. The ambient conditions correspond to a neutrally ($\theta = 300$ K) stratified dry atmosphere with air initially at rest (see Straka et al, 1993 for details on the reference conditions). Kinematic viscosity is imposed to $\nu_f = 0.1$ $m^2.s^{-1}$. The case satisfies the incompressible or quasi-incompressible hypothesis (low Mach number). The two-dimensional domain is defined by $x \in [0 : 51, 2.10^3]$ m in the horizontal direction and $z \in [0 : 6, 4.10^3]$ m in the vertical direction. The type of lateral boundary conditions is cyclic. Free slip conditions without permeability are applied at the bottom and top surfaces. No relaxation (to avoid reflective waves) is injected in the upper part of the atmosphere. The flow is symmetric with respect to the z axis at $x = 25, 6.10^3$ m (hence only the results in the region $x > 25, 6.10^3$ m are shown). Absolute temperature is initially placed in a region with an elliptic shape and maximum amplitude localized in its center: Location are $(x_c; z_c) = (25, 6; 3).10^3$ m; size is $(x_r; z_r) = (4; 2).10^3$ m; region is $R = \sqrt{(\frac{x-x_c}{x_r})^2 + (\frac{z-z_c}{z_r})^2}$; amplitude is $\Delta T = -15cos(\pi R + 1)/2$ K if $R < 1$, $\Delta T = 0$ K elsewhere.

After nine minutes the shear at the front (between the disturbed and undisturbed region) is sufficiently high to initiate a vortex shedding (Kelvin-Helmholtz instability type). After fifteen minutes three vortices are clearly visible. Here we only focus on the flow properties at this particular time. The variables obtained at $t = 900$ s are presented in the Table S1.

Front location	$x_{front} = x - 25600$
Extreme values of the temperature	$\Delta\theta_{min} = \theta_{min} - 300$
Extreme values of the velocity field	$u_{min,max}$ (horizontal direction), $v_{min,max}$ (vertical direction)
Kinetic energy	$e_k = \frac{1}{2}\|\|\boldsymbol{u}\|\|^2$
Enstrophy	$e_s = (\nabla \times \boldsymbol{u})^2 = \|\|\boldsymbol{\omega}\|\|^2$

	$\Delta\theta_{min}$ K	u_{min} $m.s^{-1}$	u_{max} $m.s^{-1}$	v_{min} $m.s^{-1}$	v_{max} $m.s^{-1}$	x_{front} km	$\sum\|\|\boldsymbol{u}\|\|^2$ $m^2.s^{-2}$	$\sum\|\|\boldsymbol{\omega}\|\|^2$ $_{10^{-5}}s^{-2}$	ω_{max} $_{10^{-2}}s^{-1}$
$\Delta x = 25m$									
Rosa et al. (2011)	-9.96	-15.29	35.06	-15.94	13.07	15.16			
Straka et al. (1993)	-9.77	-15.19	36.46	-15.95	12.93	15.53	11.18	8.37	
MNH-BFM	-9.66	-15.26	36.14	-15.91	12.93	15.39	10.50	8.15	7.45
$\Delta x = 50m$									
MNH-BFM	-9.66	-15.24	36.11	-15.88	12.89	15.40	10.50	8.09	7.43
MNH-IBM	-9.74	-15.13	36.08	-15.94	13.09	15.41	10.18	7.87	7.41

Table S1. *The Straka current: definition of the studied local and integrated variables (top) and comparison (depending on the spatial resoutions) of MNH-IBM, MNH-BFM results and thus of Rosa et al. (2011) and Straka et al. (1993) (bottom).*

Results. To obtain a MNH-BFM reference solution a 2048×256 mesh ($\Delta x_{ref} = 25$ m) is used. The time step is fixed to $\Delta t = 0.1$ s: the CFL number respects $\frac{U_{max}\Delta t}{\Delta x} < 0.2$. The results of the MNH-BFM reference solution are in good agreement with those of Straka et al. (1993) and Rosa et al. (2011) using the same spatial resolution: the travelled distance by the current, the energies and the vorticity production are well-recovered (Table S1).

Using a 1024×128 mesh ($\Delta x_{ref} = 50$ m) and $\Delta t = 0.1$ s ($\frac{U_{max}\Delta t}{\Delta x} < 0.1$), the case is simulated with MNH-BFM and MNH-IBM. The convergence in space of the solution is shown by the weak differences of the MNH-BFM results between the $\Delta x_{ref} = 25$ m and $\Delta x_{ref} = 50$ m resolutions. The good agreement beteen MNH-BFM and MNH-IBM on the density current location and its characteristics at $t = 900$ s is illustrated in Figure F1 plotting the θ potential temperature (top), the kinetic energy (middle) and the enstrophy (bottom) contours (BFM in blue line; IBM in red line). Note that two additional points are necessary in the vertical direction (below the ground, dashed line in Figure F1) to compute the ghost points in MNH-IBM.

Even if the fluid-solid interface is flat in this case, MNH-IBM preserves the change of the potential energy due to the gravitational acceleration in the momemtum equation, which reflects the impermeability conditions of the ground due to the Cut-Cell Technique employed in the pressure solver. The slip condition on the tangent velocity and the potential temperature at the ground are also well-insured by the Ghost-Cell Technique.

References

Lac, C., Chaboureau, J.-P., Masson, V., Pinty, J.-P., Tulet, P., Escobar, J., Leriche, M., and others: Overview of the Meso-NH model version 5.4 and its applications. Geosci. Model Dev., 11, 1929-1969, 2018.

Lafore, J. P., Stein, J., Asencio, N., Bougeault, P., Ducrocq, V., Duron, J., Fisher, C., Hèreil, P., Mascart, P., Masson, V., Pinty, J. P., Redelsperger, J.-L., Richard, E., and Vilà-Gueau de Arellano, J.: The Meso-NH Atmospheric Simulation System. Part I: adiabatic formulation and control simulations. Scientific objectives and experimental design. Annales Geophysicae, 16, 90-109, 1998.

Lunet, T., Lac, C., Auguste, F., Visentin, F., Masson, V., and Escobar, J.: Combination of WENO and explicit Runge-Kutta methods for wind transport in Meso-NH model. Mon. Wea. Rev., 145(9), 3817-3838, 2017.

Rosa, B., Kurowski, M., and Ziemiański, M.: Testing the anelastic nonhydrostatic model EULAG as a prospective dynamical core of a numerical weather prediction model Part I: Dry benchmarks. Acta Geophysica, 6(59), 1236-1266, 2011.

Straka, JM, Wilhelmson, R. B., Wicker, L. J., Anderson, J. R., and Droegemeier, K. K.: Numerical solutions of a non-linear density current: A benchmark solution and comparisons. Int. J. for Num. Methods in Fluids, 17(1), 1-22, 1993.